


# Optical Transparency and Local Electronic Structure of Yb-Doped $\text{Y}_2\text{O}_3$ Ceramics with Tetravalent Additives

Ivan S. Zhidkov <sup>1,\*</sup> , Andrey I. Kukharensky <sup>1</sup>, Roman N. Maksimov <sup>2,3</sup>, Larisa D. Finkelstein <sup>4</sup>, Seif O. Cholakh <sup>1</sup>, Vladimir V. Osipov <sup>2</sup> and Ernst Z. Kurmaev <sup>1,4</sup>

<sup>1</sup> Institute of Physics and Technology, Ural Federal University, Mira Str. 19, 620002 Yekaterinburg, Russia; a.i.kukharensky@urfu.ru (A.I.K.); s.o.cholakh@urfu.ru (S.O.C.); ernst.kurmaev@gmail.com (E.Z.K.)

<sup>2</sup> Institute of Electrophysics, Ural Branch of Russian Academy of Sciences, Amundsen Str. 106, 620016 Yekaterinburg, Russia; romanmaksimov@e1.ru (R.N.M.); osipov@iep.uran.ru (V.V.O.)

<sup>3</sup> SEC “Nanomaterials and nanotechnologies”, Ural Federal University, 620002 Yekaterinburg, Russia

<sup>4</sup> M.N. Mikheev Institute of Metal Physics, Ural Branch of Russian Academy of Sciences, S. Kovalevskoi Str. 18, 620108 Yekaterinburg, Russia; nechkina@ifmlrs.uran.ru

\* Correspondence: i.s.zhidkov@urfu.ru

Received: 30 January 2019; Accepted: 14 February 2019; Published: 16 February 2019



**Abstract:** The results of optical transmission and X-ray core-level spectra measurements of Yb:Y<sub>2</sub>O<sub>3</sub> ceramics with different tetravalent sintering additives (ZrO<sub>2</sub>, CeO<sub>2</sub> and HfO<sub>2</sub>) fabricated from nanopowders (produced by the laser ablation method) and then annealed at 1400 °C in air for 2 h are presented. It is found that the transmission values for ZrO<sub>2</sub>- and HfO<sub>2</sub>-doped ceramics at the lasing wavelengths are higher than those of CeO<sub>2</sub>-doped samples. The X-ray photoelectron spectra (XPS) O 1s spectra show that the relative intensity of oxygen defect peak detected for 3Yb:Y<sub>2</sub>O<sub>3</sub> + 5CeO<sub>2</sub> ceramics decreases substantially and consistently compared to that of 5Yb:Y<sub>2</sub>O<sub>3</sub> + 5HfO<sub>2</sub> and 3Yb:Y<sub>2</sub>O<sub>3</sub> + 5ZrO<sub>2</sub> samples. This can be attributed to a more complete filling of oxygen vacancies due to annealing-induced oxygen diffusion into the highly defective sintered ceramics. The measurements of XPS Ce 3d spectra showed that the insufficiently complete filling of the oxygen vacancies in the 3Yb:Y<sub>2</sub>O<sub>3</sub> + 5CeO<sub>2</sub> compound is due to the appreciable presence of trivalent cerium ions.

**Keywords:** yttrium oxide; ceramic; electronic structure; X-ray photoelectron spectra (XPS); transmission; annealing

## 1. Introduction

In recent decades the transparent Y<sub>2</sub>O<sub>3</sub> ceramic has attracted interest due to its unique combination of properties, such as broad transparency range (0.2–8 μm), high thermal conductivity (approximately 13.6 W/mK), high solubility of trivalent rare-earth ions and a relatively low cut-off phonon energy (380 cm<sup>−1</sup>) [1,2]. The transparent Y<sub>2</sub>O<sub>3</sub> ceramic can be considered as a good alternative to single-crystal materials with a high melting point (2430 °C), and the phase transition point is approximately 2280 °C [3]. At the same time, its high melting point causes the addition of several special additives to the initial yttrium oxide, such as ThO<sub>2</sub>, CeO<sub>2</sub>, HfO<sub>2</sub>, and ZrO<sub>2</sub>, which should reduce the sintering temperature [4,5]. It was found that in the process of vacuum sintering, Y<sub>2</sub>O<sub>3</sub> ceramics with tetravalent additives lose their transparency due to the darkening of color [6], which can significantly limit the potential applications. It is believed that this is due to oxygen atoms that escape from the doped Y<sub>2</sub>O<sub>3</sub> lattice and form oxygen vacancy defects [7], which give rise to the formation of F and F<sup>+</sup> centers in the wide band gap. It is known that such oxygen vacancies in sintered ceramics can be easily removed by post-annealing in an oxygen atmosphere or in air [8–10]. At the same time, the question of the influence of such processing not only on the optical properties of ceramics but also on the valence state

of impurity ions remains open. In particular, in our previous paper we studied the influence of time of annealing in air (from 1 to 10 h at 1400 °C) on optical properties and X-ray photoelectron spectra (XPS) of  $\text{Y}_2\text{O}_3$  ceramics doped with 5 mol%  $\text{CeO}_2$  [11]. It was shown that measurements of XPS spectra make it possible to estimate the contribution of defects related to oxygen and optical transparency, as well as the effect of different calcination modes on the state of Ce ions. However, the effect of various technological additives on the final laser ceramics containing rare-earth ions may not be the same. In the present paper, the annealing conditions were fixed (1400 °C, 2 h) whereas the type of tetravalent additives was varied ( $\text{ZrO}_2$ ,  $\text{CeO}_2$  and  $\text{HfO}_2$ ) and the optical transparency and local atomic electronic structure were studied in  $\text{Yb}:\text{Y}_2\text{O}_3$  ceramics.

## 2. Materials and Methods

As initial materials, commercial high-purity powders  $\text{Y}_2\text{O}_3$ ,  $\text{Yb}_2\text{O}_3$  (>99.99% TREO, Lanthit, Moscow, Russia),  $\text{ZrO}_2$ ,  $\text{HfO}_2$  and  $\text{CeO}_2$  (>99%, Lanthit, Moscow, Russia) were used. For the preparation of 3 and 5 at.% Yb-doped samples, pure  $\text{Y}_2\text{O}_3$  was dry-mixed with different tetravalent additives (5 mol%  $\text{ZrO}_2$ ,  $\text{HfO}_2$  or  $\text{CeO}_2$ ) for 24 h in a rotary mixer with an inclined axis of rotation. Then, in order to produce laser targets, these mixtures were compacted at a pressure of 10 MPa and pre-sintered at 1300 °C for 5 h in air. No charge compensation admixture was used. Finally, the obtained targets were ablated by radiation from a pulse-periodical  $\text{CO}_2$  laser LAERT ( $\lambda = 10.6 \mu\text{m}$ ) for producing nanopowders [12]. The synthesized nanoparticles with different chemical compositions were annealed in air at 1100 °C for 3 h in order to convert them from a metastable monoclinic phase into the main cubic phase. The annealed nanopowders were uniaxially pressed at 200 MPa into disks with a 15-mm diameter. At the next step, removing the organic components was carried out by calcining at 800 °C for 3 h, then the green disks were sintered at 1780 °C for 20 h under a  $10^{-3}$ -Pa vacuum. The ceramic samples were then annealed at 1400 °C for 2 h. Samples were mirror-polished on both surfaces.

The structure of samples was characterized by X-ray diffraction (XRD) using a D8 Discover apparatus. A typical XRD pattern ( $3\text{Yb}:\text{Y}_2\text{O}_3 + 5\text{ZrO}_2$ ) is shown in Figure 1. Samples were well crystallized and coincided with a cubic  $\text{Y}_2\text{O}_3$  phase. It was found that the addition of tetravalent additives had a small effect on the crystal structure. For example, in the case of  $\text{HfO}_2$  and  $\text{ZrO}_2$ , the lattice parameter decreased slightly with the content of additives (from 1.0613 nm to 1.0605 nm).

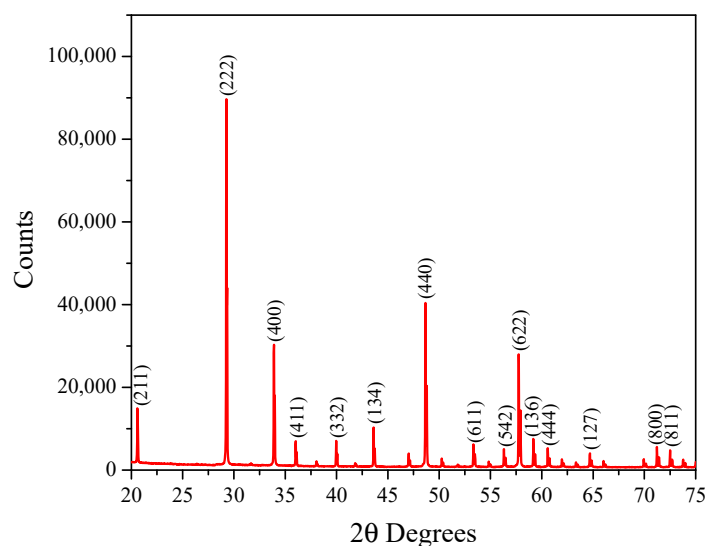


**Figure 1.** Typical X-ray diffraction (XRD) patterns of the  $\text{Yb}:\text{Y}_2\text{O}_3$  ceramics.

The transmission spectra of the ceramics were measured at room temperature with a Shimadzu UV-1700 spectrophotometer (Shimadzu Corp., Kyoto, Japan) operating at a 200–1100 nm wavelength range.

High-resolution core-level X-ray photoelectron spectra were obtained using a PHI 5000 VersaProbe spectrometer (ULVAC Physical Electronics, Chanhassen, MN, USA). This spectrometer was based on a classic X-ray optic scheme with a quartz monochromator and a hemispherical energy analyzer (binding energy range are from 0 to 1500 eV). The device was equipped with electrostatic focusing and magnetic screening and the energy resolution was about 0.5 eV. Pumping of the analytical chamber was carried out using an ion pump providing residual pressure better than  $10^{-7}$  Pa. The XPS spectra were recorded using monochromatic Al K $\alpha$  X-ray emission (1486.6 eV); the spot size was 200  $\mu$ m. In order to avoid surface contamination (due to polishing), all samples were freshly cleaved before XPS measurements. The device was equipped with electrostatic focusing and magnetic screening and the energy resolution was about 0.5 eV. Finally, the spectra were processed using ULVAC-PHI MultiPak Software 9.8. The XPS background was calculated according to the Shirley method.

### 3. Results and Discussion

Optical transmission spectra of Yb:Y<sub>2</sub>O<sub>3</sub> ceramics with different tetravalent additives are shown in Figure 2. It was found that at lasing wavelengths (1030–1080 nm), the ceramics doped with ZrO<sub>2</sub> and HfO<sub>2</sub> had higher transmission values than those for the ceramics doped with CeO<sub>2</sub>. However, the spectral characteristics of the absorption edge were different for samples under study. The “orange peel” effect appeared less visible to the naked eye for ZrO<sub>2</sub>-doped sample than for HfO<sub>2</sub> and CeO<sub>2</sub>-doped samples. Thus, we can conclude that samples doped with ZrO<sub>2</sub> are better suited for the fabrication of highly transparent yttria ceramics.

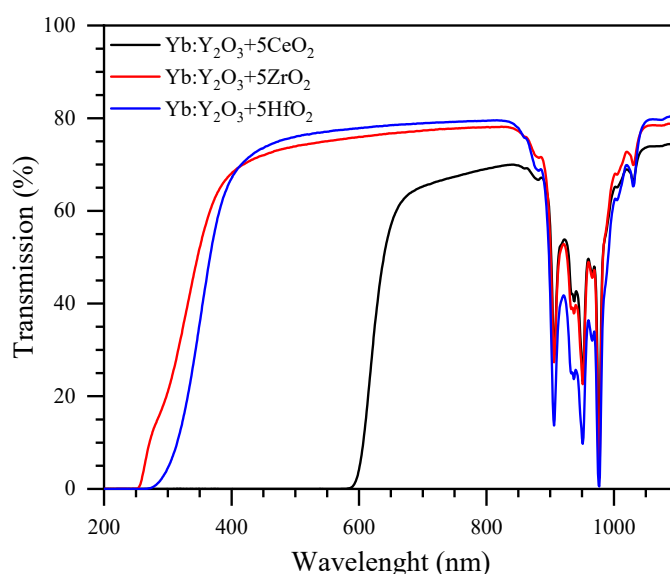


**Figure 2.** Transmission spectra of Yb:Y<sub>2</sub>O<sub>3</sub> ceramics with different tetravalent sintering additives.

The XPS survey spectra (Figure 3) did not show the presence of any uncontrolled impurities, which evidences the high quality of the samples under investigation. The surface composition determined from these spectra is presented in Table 1. One can see from this table that the O/Y ratio for 3Yb:Y<sub>2</sub>O<sub>3</sub> + 5CeO<sub>2</sub> (1.88) was less than that of 5Yb:Y<sub>2</sub>O<sub>3</sub> + 5HfO<sub>2</sub> (1.93) and 3Yb:Y<sub>2</sub>O<sub>3</sub> + 5ZrO<sub>2</sub> (1.96).

**Table 1.** Surface composition (in at.%).

Sample	C	O	Y	Yb	Hf	Zr	Ce	O/Y
3Yb:Y <sub>2</sub> O <sub>3</sub> + 5CeO <sub>2</sub>	39.1	38.9	20.6	1.6	–	–	0.2	1.88
5Yb:Y <sub>2</sub> O <sub>3</sub> + 5HfO <sub>2</sub>	44.9	35.1	18.1	1.3	0.6	–	–	1.93
3Yb:Y <sub>2</sub> O <sub>3</sub> + 5ZrO <sub>2</sub>	42.4	37.0	18.8	1.4	–	0.4	–	1.96

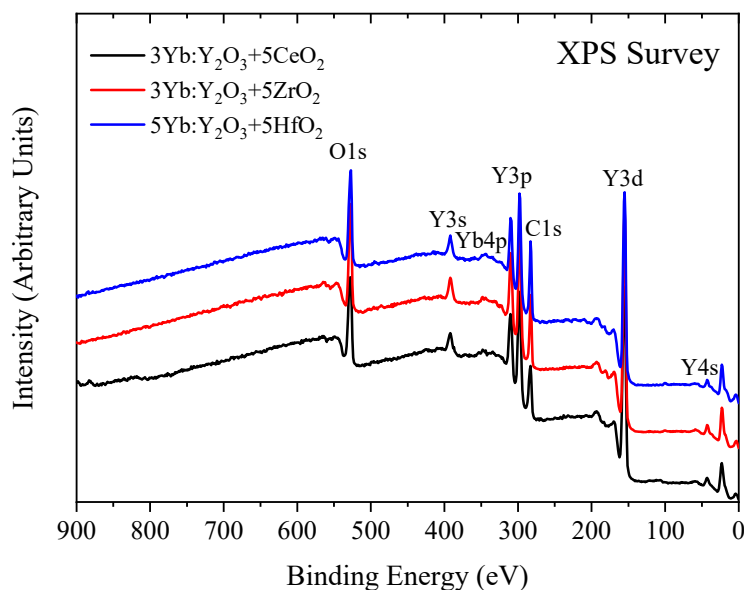


**Figure 3.** X-ray photoelectron spectra (XPS) survey of Yb:Y<sub>2</sub>O<sub>3</sub> ceramics with tetraivalent additives.

The measurements of high-energy resolved XPS O 1s spectra (Figure 4) show the contributions of O1—lattice oxygen (529.4 eV), O2—absorbed oxygen (531.8 eV) and O3—oxygen defects (530.4 eV) [13,14]. One can see from the deconvoluted spectra that the contribution of defect oxygen was consequently decreased from 3Yb:Y<sub>2</sub>O<sub>3</sub> + 5CeO<sub>2</sub> (Figure 4a) to 5Yb:Y<sub>2</sub>O<sub>3</sub> + 5HfO<sub>2</sub> (Figure 4b) and to 3Yb:Y<sub>2</sub>O<sub>3</sub> + 5ZrO<sub>2</sub> (Figure 4c). The decrease in the defect oxygen content (O3) is remarkably correlated with an increase in the optical transmission in this series of compounds (see Figure 2), as well as with an increase in the O/Y ratio measured from the survey spectra (Table 1). In this connection, it is of interest to study the core-level spectra of additives and to determine, with their help, the corresponding cation oxidation states.

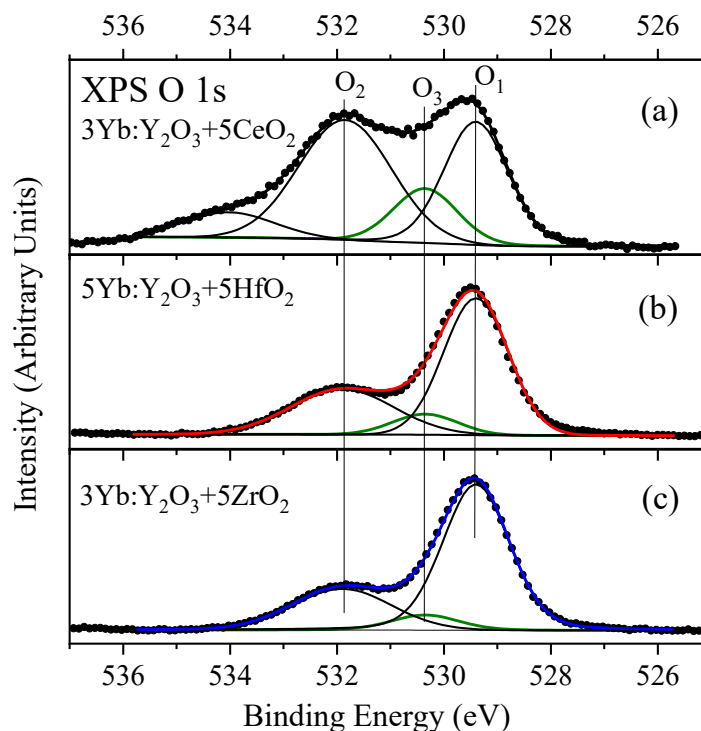


**Figure 4.** XPS O 1s spectra of Yb:Y<sub>2</sub>O<sub>3</sub> ceramics with tetraivalent additives: (a) 3Yb:Y<sub>2</sub>O<sub>3</sub> + 5CeO<sub>2</sub>; (b) 5Yb:Y<sub>2</sub>O<sub>3</sub> + 5HfO<sub>2</sub>; (c) 3Yb:Y<sub>2</sub>O<sub>3</sub> + 5ZrO<sub>2</sub>.

The high-energy resolved XPS Zr 3d and Hf 4f spectra of 3Yb:Y<sub>2</sub>O<sub>3</sub> + 5ZrO<sub>2</sub> and 5Yb:Y<sub>2</sub>O<sub>3</sub> + 5HfO<sub>2</sub> are given in Figure 5. Unfortunately, the XPS Zr 3d spectra overlap strongly with the Yb 4d spectra (Figure 5a), and the XPS Hf 4f spectra with the XPS O 2s spectra, which makes it impossible to determine the contributions of trivalent ions whose small inputs could be expected from a finite amount of defective oxygen in 3Yb:Y<sub>2</sub>O<sub>3</sub> + 5ZrO<sub>2</sub> and 5Yb:Y<sub>2</sub>O<sub>3</sub> + 5HfO<sub>2</sub> (Figure 4b,c). The binding energy of the XPS Zr 3d spectrum (184.0 eV) for 3Yb:Y<sub>2</sub>O<sub>3</sub> + 5ZrO<sub>2</sub> (Figure 5a) was close to that of tetravalent zirconium [15]. The corresponding energy of XPS Hf 4f<sub>7/2</sub> spectrum of 5Yb:Y<sub>2</sub>O<sub>3</sub> + 5HfO<sub>2</sub> was found to be the same as that for HfO<sub>2</sub> (16.7 eV) [13].

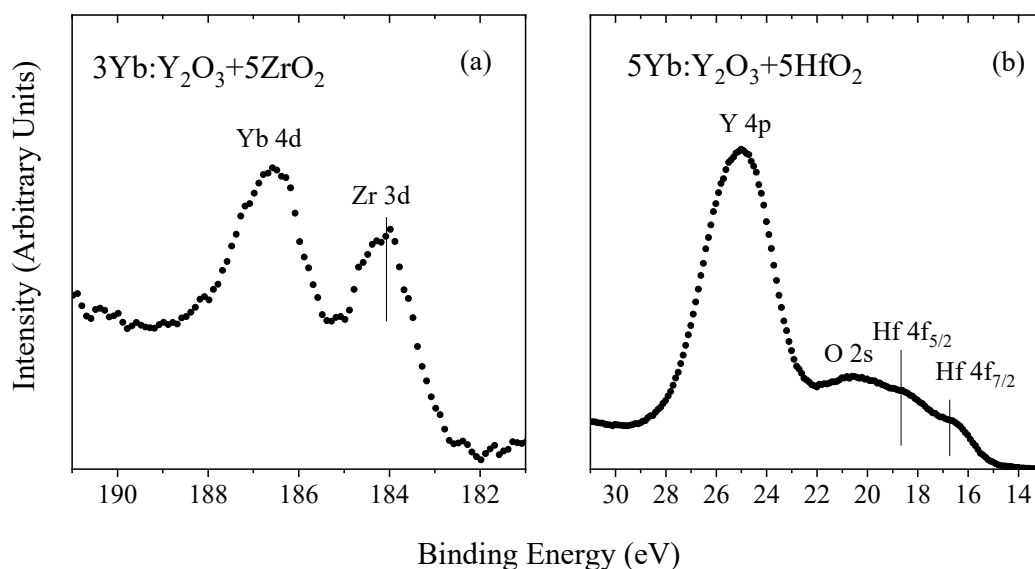


**Figure 5.** XPS spectra of Yb:Y<sub>2</sub>O<sub>3</sub> ceramics with tetravalent additives: (a) Zr 3d; (b) Hf 4f.

The XPS Ce 3d spectra of 3Yb:Y<sub>2</sub>O<sub>3</sub> + 5CeO<sub>2</sub> ceramics are given in Figure 6. For comparison, the spectra of reference samples CeO<sub>2</sub> and Ce<sub>2</sub>O<sub>3</sub> [16] are shown in the same figure. Let us consider the structure of Ce 3d spectra of reference compounds Ce<sub>2</sub>O<sub>3</sub> and CeO<sub>2</sub>. When the 3d core level is ionized, the final state is a spin-orbit doublet of 3d<sub>5/2</sub> (with lower binding energy) and 3d<sub>3/2</sub> (with higher binding energy). The structure of each of the terms of the spin-doublet is determined by the electric potential of the X-ray 3d-hole interacting with the excited states, which are attracted by the system for its relaxation after 3d-ionization. For Ce<sup>3+</sup> and Ce<sup>4+</sup> ions the initial states are different (*f*<sup>1</sup> and *f*<sup>0</sup> states, respectively), so the final states also differ. In Ce<sup>3+</sup>, each of the spin-doublet terms consists of two lines: *v*<sup>0</sup> and *v*<sup>1</sup> in 3d<sub>5/2</sub>; *u*<sup>0</sup> and *u*<sup>1</sup> in 3d<sub>3/2</sub>. Lines *v*<sub>0</sub> and *u*<sub>0</sub> correspond to the relaxed final state containing the *f*<sup>2</sup> configuration, and *v* and *u* to unrelaxed states with the *f*<sup>1</sup> configuration coinciding with the unexcited (initial) one. For Ce<sup>4+</sup>, *v* and *u* lines correspond to the relaxed final state containing the *f*<sup>2</sup> configuration, *v*<sup>1</sup> and *u*<sup>1</sup> to the partially relaxed state with the *f*<sup>1</sup> configuration and *v*<sup>0</sup> and *u*<sup>0</sup> to the unrelaxed state with the *f*<sup>0</sup> configuration coinciding with the initial state [17].

According to [18], a quantitative analysis of the concentration of Ce<sup>3+</sup> ions based on measured XPS Ce 3d-spectra can be performed using the formula:

$$[\text{Ce}^{3+}] = \frac{(A_{v_0} + A_{v'} + A_{u_0} + A_{u'})}{(A_{v_0} + A_{v'} + A_{u_0} + A_{u'} + A_v + A_{v''} + A_{v'''} + A_u + A_{u''} + A_{u'''})} \quad (1)$$

where *A<sub>i</sub>* is the integrated area of peak “i”.

Using the results of the deconvolution of XPS Ce 3d spectra given in Figure 6, we performed an analysis according to which the fraction of Ce<sup>3+</sup> in annealed 3Yb:Y<sub>2</sub>O<sub>3</sub> + 5CeO<sub>2</sub> ceramics was 34%. It is worth noting that, contrary to our previous work [11], this study reveals a much smaller amount of

cerium ions in the 3+ valence state. We believe that the presence in the ceramics of  $\text{Yb}^{3+}$  ions, which can bind a part of the defective oxygen atoms, allows some of the Ce ions to pass into the 4+ valence state.

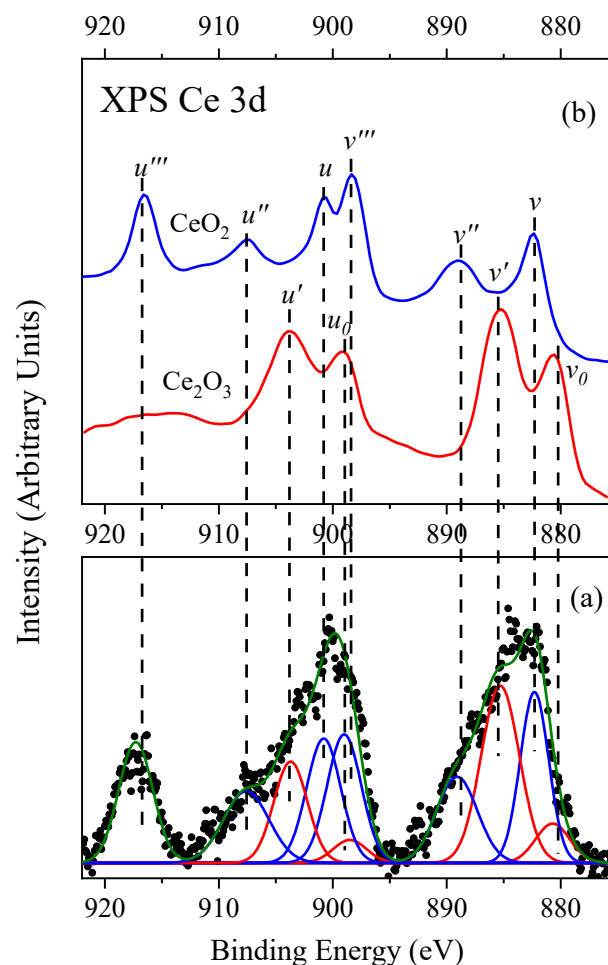


**Figure 6.** XPS Ce 3d-spectra: (a) 3Yb:Y<sub>2</sub>O<sub>3</sub>+5CeO<sub>2</sub> ceramics; (b) reference CeO<sub>2</sub> and Ce<sub>2</sub>O<sub>3</sub> [15].

The process of obtaining optically transparent yttria-based polycrystalline ceramics is quite complex and involves multiple stages. At the first stage, sufficiently pure and dense (pore-free) ceramics must be obtained, which is usually achieved by sintering in vacuum (to reduce the sintering temperature, the tetravalent additives to Y<sub>2</sub>O<sub>3</sub> are used). However, after sintering in vacuum, the final product shows a black color or a so-called discoloration. This discoloration is associated with the formation of oxygen vacancies in ceramics induced by reducing conditions in a vacuum, leading to the formation of F and F<sup>+</sup> centers in a wide band gap [19]. On the one hand, the post-annealing of sintered ceramics in air or an oxygen atmosphere decreases the number of oxygen vacancies. On the other hand, it is difficult to completely eliminate the oxygen vacancies perfectly, preventing the development of pores during the post-annealing, and the optical characteristics are inevitably deteriorated. In this situation, the control over the formation of oxygen vacancies and changes in their content, depending on the conditions of synthesis, becomes of particular importance. It was shown in [20] that this control can be performed indirectly by measuring the paramagnetic resonance spectra, which show the presence of trivalent hafnium and zirconium ions in Yb:Y<sub>2</sub>O<sub>3</sub> + 6HfO<sub>2</sub> and Yb:Y<sub>2</sub>O<sub>3</sub> + 6ZrO<sub>2</sub>. In the present paper, it is shown that the relative content of defective oxygen can be determined directly by measuring X-ray photoelectron O 1s spectra, which allows for choosing the most optimal annealing conditions to obtain the maximum optical transparency of ceramics.



#### 4. Conclusions

It was found that the optical transparency of Yb:Y<sub>2</sub>O<sub>3</sub> ceramics depends on the type of sintering additive. The composition of Yb:Y<sub>2</sub>O<sub>3</sub> + 5ZrO<sub>2</sub> demonstrates the best transparency from the point of view of its use as laser ceramics. This effect is confirmed by measurements of XPS spectra. It was shown that the peak of oxygen defects in the O 1s spectrum decreases in the series CeO<sub>2</sub> → HfO<sub>2</sub> → ZrO<sub>2</sub>, which was also confirmed by the Y/O concentration ratio. In addition, it was shown that the Zr and Hf ions are in the 4+ state, while in the 3Yb:Y<sub>2</sub>O<sub>3</sub> + 5CeO<sub>2</sub> ceramics both Ce<sup>4+</sup> ions and Ce<sup>3+</sup> ions are present. In conclusion, we assume that the correlation of all the indicated spectra suggests that measurements of the O 1s spectra can serve as an indicator for choosing the optimal synthesis modes for the most optically transparent laser ceramics.

**Author Contributions:** I.S.Z., E.Z.K. and V.V.O. conceived and designed the experiments; I.S.Z., A.I.K. and R.N.M. performed the experiments; I.S.Z., A.I.K., L.D.F. S.O.C. and E.Z.K. analyzed the data; R.N.M. and V.V.O. contributed materials/analysis tools; I.S.Z., L.D.F. and E.Z.K. wrote the paper.

**Funding:** This study was supported by FASO (Theme “Electron” No. AAAA-A18-118020190098-5). The XPS measurements were supported by the Ministry of Education and Science of the Russian Federation (Project No. 3.7270.2017/8.9) and the Government of the Russian Federation (Act 211, agreement No. 02.A03.21.0006). Fabrication of ceramic samples was performed in the framework of the state task of IEP UB RAS.

**Conflicts of Interest:** The authors declare no conflict of interest.

#### References

- Li, J.; Pan, Y.-B.; Zeng, Y.-P.; Liu, W.-B.; Jiang, B.-X.; Guo, J.-K. The history, development, and future prospects for laser ceramics: a review. *Int. J. Refract. Met. Hard Mater.* **2013**, *39*, 44–52. [\[CrossRef\]](#)
- Zhu, L.-L.; Park, Y.-J.; Gan, L.; Kim, H.-N.; Ko, J.-W.; Kim, H.-D. Fabrication of transparent Y<sub>2</sub>O<sub>3</sub> ceramics with record-high thermal shock resistance. *J. Eur. Ceram. Soc.* **2018**, *38*, 4050–4056. [\[CrossRef\]](#)
- Lu, J.-R.; Takaichi, K.; Uematsu, T.; Shirakawa, A.; Musha, M.; Ueda, K.; Yagi, H.; Yanagitani, T.; Kaminskii, A.A. Yb<sup>3+</sup>: Y<sub>2</sub>O<sub>3</sub> ceramics – a novel solid-state laser material. *Jpn J. Appl. Phys.* **2012**, *41*, L1373–L1375. [\[CrossRef\]](#)
- Cheng, X.; Yuan, C.; Green, N.R.; Withey, P.A. Sintering mechanisms of yttria with different additives. *Ceram. Int.* **2013**, *39*, 4791–4799.
- Osipov, V.V.; Shitov, V.A.; Maksimov, R.N.; Solomonov, V.I. Properties of transparent Re<sup>3+</sup>: Y<sub>2</sub>O<sub>3</sub> ceramics doped with tetravalent additives. *Opt. Mater.* **2015**, *50*, 65–70. [\[CrossRef\]](#)
- Tsukuda, Y. Properties of black Y<sub>2</sub>O<sub>3</sub> sintered bodies. *Mater. Res. Bull.* **1981**, *16*, 453–459. [\[CrossRef\]](#)
- Li, X.; Mao, X.; Feng, M.; Xie, J.; Jiang, B.; Zhang, L. Optical absorption and mechanism of vacuum-sintered ZrO<sub>2</sub>-doped Y<sub>2</sub>O<sub>3</sub> ceramics. *J. Eur. Ceram. Soc.* **2016**, *36*, 4181–4184. [\[CrossRef\]](#)
- Zhang, W.; Lu, T.; Wei, N.; Ma, B.; Li, F.; Lu, Z.; Qi, J. Effect of annealing on the optical properties of Nd:YAG transparent ceramics. *Opt. Mater.* **2012**, *34*, 685–690. [\[CrossRef\]](#)
- An, L.; Ito, A.; Goto, T. Effects of Sintering and Annealing Temperature on Fabrication of Transparent Lu<sub>2</sub>Ti<sub>2</sub>O<sub>7</sub> by Spark Plasma Sintering. *J. Am. Ceram. Soc.* **2011**, *94*, 3851–3855. [\[CrossRef\]](#)
- Gan, L.; Park, Y.-J.; Kim, H.-N.; Kim, J.-M.; Ko, J.-W.; Lee, J.-W. Effects of presintering and annealing on the optical transmittance of Zr-doped Y<sub>2</sub>O<sub>3</sub> transparent ceramics fabricated by vacuum sintering conjugated with post-hot-isostatic pressing. *Ceram. Int.* **2015**, *41*, 9622–9627.
- Zhidkov, I.S.; Maksimov, R.N.; Kukharensko, A.I.; Finkelstein, L.D.; Cholakh, S.O.; Osipov, V.V.; Kurmaev, E.Z. Influence of post-annealing in air on optical and XPS spectra of Y<sub>2</sub>O<sub>3</sub> ceramics doped with CeO<sub>2</sub>. *Mendeleev Commun.* **2019**, *29*, 102–104. [\[CrossRef\]](#)
- Osipov, V.V.; Kotov, Yu.A.; Ivanov, M.G.; Samatov, O.M.; Lisenkov, V.V.; Platonov, V.V.; Murzakaev, A.M.; Medvedev, A.I.; Azarkevich, E.I. Laser synthesis of nanopowders. *Las. Phys.* **2006**, *16*, 116–125. [\[CrossRef\]](#)
- Moulder, J.F.; Stickle, W.F.; Sobol, P.F.; Bomben, K.D. *Handbook of X-ray Photoelectron Spectroscopy*; Physical Electronic Division: Eden Prairie, MN, USA, 1995.
- Hu, Y.; Li, Z.; Pan, W. Sandwich-like transparent ceramic demonstrates ultraviolet and visible broadband downconversion luminescence. *RSC Adv.* **2018**, *8*, 13200–13204. [\[CrossRef\]](#)

15. Lung, C.Y.K.; Kukk, E.; Hägerth, T.; Matinlinna, J.P. Surface modification of silica-coated zirconia by chemical treatments. *Appl. Surf. Sci.* **2010**, *257*, 1228–1235. [[CrossRef](#)]
16. Mullins, D.R.; Overbury, S.H.; Huntley, D.R. Electron spectroscopy of single crystal and polycrystalline cerium oxide surfaces. *Surf. Sci.* **1998**, *409*, 307–319. [[CrossRef](#)]
17. Kotani, A.; Jo, T.; Parlebas, J.C. Many-body effects in core-level spectroscopy of rare-earth compounds. *Adv. Phys.* **1998**, *37*, 37–85. [[CrossRef](#)]
18. Deshpande, S.; Patil, S.; Kuchibhatla, S.V.N.T.; Seal, S. Size dependency variation in lattice parameter and valency states in nanocrystalline cerium oxide. *Appl. Phys. Lett.* **2005**, *87*, 133113–133115. [[CrossRef](#)]
19. Jung, W.K.; Ma, H.J.; Park, Y.; Kim, D.K. A robust approach for highly transparent  $Y_2O_3$  ceramics by stabilizing oxygen defects. *Scripta Mater.* **2017**, *137*, 1–4. [[CrossRef](#)]
20. Osipov, V.V.; Solomonov, V.I.; Konev, S.F.; Cholakh, S.O. Trivalent Zirconium and Hafnium Ions in Yttria-Based Transparent Ceramics. *Tech. Phys. Lett.* **2013**, *39*, 377–379. [[CrossRef](#)]



© 2019 by the authors. Licensee MDPI, Basel, Switzerland. This article is an open access article distributed under the terms and conditions of the Creative Commons Attribution (CC BY) license (<http://creativecommons.org/licenses/by/4.0/>).